A&A 402, 1061–1071 (2003)
DOI: 10.1051/0004-6361:20030209

Astronomy & Astrophysics

Spectroscopic analysis of two CH subgiant stars: HD 50264 and HD 87080⋆,⋆⋆

C. B. Pereira[1,2] and S. Junqueira[1]

[1] Observatório Nacional-MCT, Rua José Cristino, 77, CEP 20921-400, São Cristóvão, Rio de Janeiro-RJ, Brazil
[2] CENTRA, Instituto Superior Técnico, Avenida Rovisco Pais 1, 1096, Lisboa, Portugal

Received 23 April 2002 / Accepted 17 January 2003

Abstract. We present the abundance pattern of two CH subgiant stars HD 50264 and HD 87080 based on high-resolution optical spectra. We also determined the spectroscopic stellar atmospheric parameters, temperature and microturbulent velocity as well as stellar surface gravity from a solution of excitation and ionization equilibria of Fe I and Fe II lines under the assumption of local thermodynamic equilibrium. The abundance analysis reveals HD 50264 with a metallicity of [Fe/H] = −0.34 and HD 87080 with a metallicity of [Fe/H] = −0.51.
We compare the abundance pattern with abundances of disk stars and also with other stars of the same class. We found that iron group, α-elements, manganese, as well as sodium and aluminum of HD 50264 and HD 87080 follow the abundance pattern of the disk stars. The heavy-element abundance pattern of both stars shows enhancements by a factor of 4–6 with respect to the sun. By heavy-element we mean the elements that have been synthesized by neutron capture, such as barium, yttrium and zirconium. We also discuss the abundances of the s-process elements and compare our results with other binary systems that display enrichment due to neutron-capture reactions, through several diagrams involving the index [hs/ls] and [s/Fe], the metallicity and [C/Fe] ratio. We compare the observed abundance of the heavy elements with theoretical nucleosynthesis calculations. This shows that the s-process are best fit by models in which the seed nuclei are exposed to single neutron irradiation and with a neutron exposure of $\tau = 0.9$ and $\tau = 1.0$ respectively for HD 50264 and HD 87080. We also use the [Rb/Zr] ratio in order to investigate how this ratio behaves versus metallicity for other binary systems, including HD 50264 and HD 87080 that are s-process enriched.

Key words. stars: chemically peculiar – stars: abundances

1. Introduction

Barium giant stars ("classical barium stars") and CH subgiant represent a class of chemically peculiar stars that shows enhancement of carbon and heavy elements produced by s-process neutron-capture reactions. The former has spectral types G and K with low luminosities, $M_v \sim 0.0$, (Jaschek et al. 1985) and their position on the HR diagram is the same as the first ascent giant stars. The latter are warmer than the classical barium stars, having spectral types F-G with even lower luminosities, $M_v \sim +2.0$ (Bond 1974). Since s-process enhancements are thought to happen in stars on the thermally pulsating phase on the asymptotic giant branch (TP-AGB) and then with luminosities of $M_v \sim -3$ to -5 (Iben & Renzini 1983) such overabundance seen in barium stars remained difficult to explain. This situation changed when McClure et al. (1980) and McClure (1997) discovered that barium giant and subgiant stars are all binary systems with degenerate companions. In this way, mass transfer in these binary systems was responsible for the enhancements observed in barium stars. The enhancements occurred when the primary, now a white dwarf, was on the TP-AGB.

In this work we concentrated on two CH subgiant stars not yet analyzed, HD 50264 and HD 87080 being with the main purpose to investigate the abundance pattern of the elements created by s-process nucleosynthesis as well as the other elements (iron group, α-elements). We planned to investigate s-process nucleosynthesis by the determination of the [s/Fe]- and [hs/ls]-index and also by the determination of the neutron exposure parameter τ. The determination of τ is important for the class of chemically peculiar stars enriched due to s-process nucleosynthesis (single and binaries) because it can add another constraint to help us understand what type of neutron source would exist in these stars. This will be discussed in Sect. 4.1.2.

There are several studies where both the value of τ and/or a comparison between the predicted and observed abundances of s-process elements are available. The majority of them are for the classical barium stars (Tomkin & Lambert 1983; Smith 1984; Smith & Lambert 1984; Lambert 1985, 1988; Malaney & Lambert 1988; Zacs 1994). However for the other

Send offprint requests to: C. B. Pereira, e-mail: claudio@on.br

⋆ Based on observations made with the 1.52 m telescope at the European Southern Observatory (La Silla, Chile) under the agreement with the Observatório Nacional, Brazil.

⋆⋆ Tables 1 and 2 are only available in electronic form at http://www.edpsciences.org

classes of binary systems there are only a few comparisons: CH stars (Vanture 1992c); CH subgiants (Krishnaswamy & Sneden 1985) and yellow-symbiotics (Smith et al. 1996, 1997; Pereira et al. 1998). In some of the mentioned above papers the determination of the neutron exposure was based on the calculations given by Cowley & Downs (1980). Such calculations were later recalculated using up-to-date nuclear reactions network by Malaney (1987). In this work we will compare our heavy element abundance pattern with the calculations given by Malaney (1987a,b).

As we shall see, these two stars are very similar to each other both in their observed properties as well as in their chemical abundances. In Sect. 2 we described our observations and the resolution used. In Sect. 3 we described the chemical analysis. In Sect. 4 we discuss our results, the abundance pattern of all the elements analyzed. In addition we derived the [hs/ls]- and [s/Fe]-index and also the neutron exposure parameter, τ, for these two stars and compare the values obtained with other classes of binary systems which are also s-process enriched. We also comment on the relation between the calculated abundance pattern and the standard neutron exposure models. Finally, our conclusions are given in Sect. 5.

2. Observations

The high-resolution spectra of HD 50264 and HD 87080 analyzed in this work were obtained at the 1.52 m ESO telescope of La Silla (Chile) on October 14, 2000 (HD 50264) and February 2, 2001 (HD 87080) with the FEROS (Fiberfed Extended Range Optical Spectrograph) echelle spectrograph (Kaufer et al. 1999). The FEROS spectral resolving power is $R = 48\,000$ corresponding to 2.2 pixels of 15 μm and the wavelength coverage is from 4000 Å to 9200 Å. The nominal S/N ratio was evaluated by the measurement of the rms flux fluctuation in selected continuum windows, and a typical value achieved was S/N 120–200, after 3600 s of integration time for the two objects.

3. Analysis and results

3.1. Line selection, measurement and oscillator strengths

The spectra of both stars show many atomic absorption lines of Fe I and Fe II as well as transitions due to Ca I, Na I, Mg I, Al I, Sc II, Mn I, Ti I, V I, Cr I, Co I, Ni I, Zn I, Cu I, Y II, Ba II, La II, Ce II, Nd II and Eu II. We have chosen a set of lines sufficiently unblended to yield reliable abundances. The selected lines are listed in Table 1 for the case of Fe I and Fe II, and in Table 2 for the other elements. In Table 1 we list the Fe I and Fe II lines employed in the analysis and also the lower excitation potential, χ, of the transitions, the gf-values and the measured the equivalent widths. The latter were obtained by fitting Gaussian profiles to the observed ones. The gf-values for the Fe I and Fe II lines in Table 1 were taken from Lambert et al. (1996). For the other elements the source of gf-values are given in Table 2.

3.2. Determination of the atmospheric parameters

The determination of atmospheric parameters, effective temperature ($T_{\rm eff}$), surface gravity (log g), microturbulence (ξ) and [Fe/H] (throughout, we use the notation [X/H] = $\log(N(\mathrm{X})/N(\mathrm{H}))_\star - \log(N(\mathrm{X})/N(\mathrm{H})_\odot)$ are prerequisites for determination of final abundance. The gravity was determined by forcing Fe I and Fe II to yield the same iron abundance at the selected effective temperature. The microturbulent velocity was determined by forcing the abundance determined from individual Fe I lines to show no dependence on equivalent width. The solution for the excitation equilibrium was set by the zero slope of the trend between the Fe I abundances and the excitation potential of the measured lines. The solution thus found is unique, depending only of a set of Fe I, II lines and the atmospheric model employed, and yields as a by-product the metallicity of the star [Fe/H]. The atmospheric parameters were determined in the local thermodynamic equilibrium (LTE) model atmospheres of Kurucz (1993) using the spectral analysis code MOOG (Sneden 1973). The final adopted atmospheric parameters are given Table 3.

Figures 1 and 2 show the diagrams corresponding to the abundances of the individual Fe I lines plotted against the lower excitation potential and the reduced line strength following the best parameters for HD 50264 and HD 87080 in Table 3.

The internal errors in our adopted effective temperatures ($T_{\rm eff}$) and microturbulent velocity (ξ) can be determined from the uncertainty in the slope of the Fe I abundance versus excitation-potential and Fe I versus reduced equivalent width (W_λ/λ) relation. These quantities are given in Table 3. The standard deviation in log g was set by changing this parameter around the adopted solution until the difference between Fe I and Fe II mean abundance differed by exactly one standard deviation of the [Fe I/H] mean value.

HD 50264 was first recognized as a CH subgiant in a paper of Bond (1974) and was later confirmed by North (1995) while HD 87080 was first recognized as a CH subgiant star by Lu et al. (1983) and was also confirmed by North (1995). Table 3 shows that our atmospheric parameters agree well with North's (1995) determination for these two stars. Also, our temperature determination confirms the earlier spectral classification for these stars: HD 50264; G0 (MacConnel et al. 1972), G2 (Lu et al. 1983); HD 87080; G5 (MacConnel et al. 1972), G2 (Lu et al. 1983). Both stars have already been spectrocopically and photometrically observed by Catchpole et al. (1977). HD 50264 was suspected of being metal weak and HD 87080 was classified as a "very metal weak CH star". The metallicity obtained for the two stars in this study show that they are as moderately metal deficient as most of the CH subgiant stars analyzed so far, e.g. $-0.8 \leq$ [Fe/H] ≤ -0.1. In this range of metallicities plus the relatively high velocities (Catchpole et al. 1977; McClure 1997), CH subgiants maybe considered as a mixture of Population I and Population II stars.

Our spectroscopic gravities determined from ionization equilibria agree well with the distance determination given by astrometric data (Mennessier et al. 1997). The luminosity of both stars were estimated from the relation

$$L = 4\pi\sigma R_*^2 T_{\rm eff*}^4 \quad (1)$$

Table 3. Atmospheric and physical parameters of HD 50264 and HD 87080.

	HD 50264[a]	HD 50264[b]	HD 87080[a]	HD 87080[b]
$T_{\rm eff}$	(5 800 ± 100) K	5690	(5600 ± 150) K	5400
log g	(4.2 ± 0.2) dex	4.5	(4.0 ± 0.2) dex	4.0
[Fe/H]	(−0.34 ± 0.08) dex		(−0.51 ± 0.12) dex	
ξ (km s^{-1})	(1.0 ± 0.3)		(1.2 ± 0.4)	

a: This work.
b: North (1995).

upon entering our derived $T_{\rm eff}$ and log g. It is necessary to assume a mass for both stars, and we adopted $M_* = 1.02\,M_\odot$ for HD 50264 and 0.97 $M_\odot$ for HD 87080 considering taking the turn-off masses for the 12 Gyr isochrones of Vandenberg et al. (2000) given the metallicities of the stars analyzed in this study. Although we do not know the exact age of the stars and their masses, the influence of the adopted mass on the Eq. (1) will be small.

Considering the gravity and the uncertainties obtained (Table 3), one obtains for the luminosity of HD 50264 and HD 87080 respectively, $L = 1.8\,L_\odot{}^{+1.21\,L_\odot}_{-0.27\,L_\odot}$ and $L = 2.3\,L_\odot{}^{+1.53\,L_\odot}_{-1.03\,L_\odot}$. This corresponds to $M_V = +4.0^{+0.61}_{-0.55}$ and $M_V = +3.72^{+0.63}_{-0.55}$, respectively for HD 50264 and HD 87080 assuming no bolometric correction and $M_{\rm bol\odot} = +4.64$ (Schmidt-Kaler 1982). One then enters the observed $V = 9.1$ (HD 50264) and $V = 9.5$ (HD 87080), to obtain $r = 100^{+30}_{-26}$ pc and 130^{+44}_{-30} pc, respectively, for HD 50264 and HD 87080. However, with the uncertainties of approximately 100 K and 0.2 dex in log g for both stars, these limits easily accommodate Mennessier's et al. (1997) value of 83 pc and 160 pc, respectively, for HD 50264 and HD 87080. The positions of these stars in the HR-diagram is the same as the other sample analyzed by Smith & Lambert (1986) (see their Fig. 2).

There is anoher way to check whether our spectroscopic gravities are in good agreement with the distances given by the Hipparcos parallaxes. Using for both stars 14.11 ± 1.06 mas and 7.9 ± 1.4 mas and the equation below

$$\log\left(\frac{g}{g_\odot}\right) = \log\left(\frac{M}{M_\odot}\right) + 4\,\log\left(\frac{T}{T_\odot}\right) + 0.12 + 0.4\,BC + 0.4\,V + 2\,\log(\pi) \quad (2)$$

where π is the parallax and BC is the bolometric correction, the value of log g for HD 50264 and HD 87080 is, respectively, $\log g = 4.51^{+0.11}_{-0.06}$ dex and $\log g = 4.09^{+0.13}_{-0.17}$ dex.

3.3. Abundance analysis

Abundances of chemical elements of HD 50264 and HD 87080 were determined with the local thermodynamic equilibrium (LTE) model atmosphere techniques already described previously. In brief, equivalent widths are calculated by integration through a model atmosphere and are compared with the observed equivalent widths. The calculation is repeated, changing the abundance of the element in question, until a match is achieved. The line-synthesis code MOOG was used to carry out the calculations. The results are given in Table 4 where we list the number of lines employed for each species, *n*, the standard deviation and the abundance ratio of element to iron, [X/Fe]. These ratios were based on a solar iron abundance of $\log \epsilon_\odot$ (Fe) = 7.52. The abundances of Mn I, Cu I, Rb I and Eu II based on the lines λ6021, λ5782, λ7801 and λ6645, were obtained through a spectrum synthesis technique. The synthetic spectra were broadened to match the instrumental profile. All fine-structure and hyperfine-structure components for the lines of Cu I, Mn I and Eu II were explicitly included. The gf-values for Cu I are from Koch & Richter (1968), for Mn I from Booth et al. (1983), for Eu II from Biémont et al. (1982) and for Rb I from Tomkin & Lambert (1983). Table 4 also shows the abundance obtained for these elements.

3.4. Abundance uncertainties

The uncertainties in the derived abundances for the program stars are dominated by three main sources: the gf-values, the equivalent widths measurements and the stellar parameters. The errors in the gf-values were discussed in Junqueira & Pereira (2001) and we thus refer to this paper for a detailed discussion.

The uncertainties in the abundances, due to errors in the stellar atmospheric parameters, were computed by changing these parameters by their standard errors given in Table 3 and calculating the changes incurred in the element abundances. The results of these calculations are displayed in Cols. 2 to 6 of Tables 5 and 6. We considered the errors was independent although we noted that a change of +100 K in the temperature increasead log g by +0.6 dex.

The final uncertainty of the abundance by number is found by composing quadratically the uncertainties due to atmospheric parameters, the W_λ's and the gf's. This final uncertainty is given in the seventh column of Tables 5 and 6. In the last column we quote the observed abundance dispersion among the lines for those elements with more than three available lines. These internal errors in the abundances are due to errors in the W_λ measurements, gf-values, microturbulence, $T_{\rm eff}$, log g and NLTE effects which may account for the different lines.

Tables 5 and 6 show that neutral elements are some sensitive to the temperature variations while single ionized elements are sensitive to the variations in log g. For the elements whose abundance is based on stronger lines, such as barium,

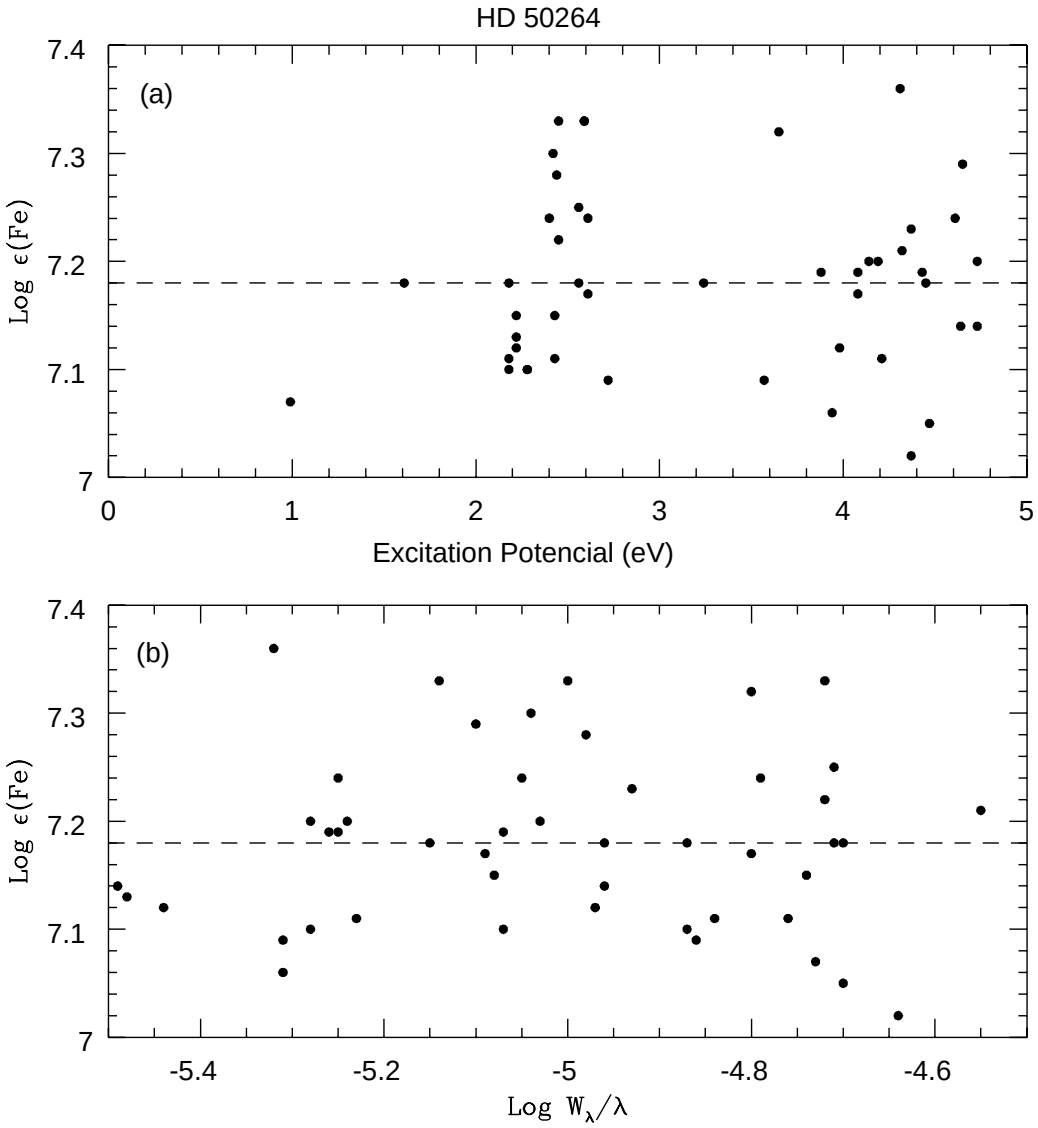

Fig. 1. The abundance of Fe by number ϵ(Fe) versus excitation potential (diagram **a)**) and the abundance of Fe by number ϵ(Fe) versus log (W_λ/λ) (diagram **b)**) for the 62 lines of Fe I,II employed in the determination of $T_{\rm eff}$, ξ and ϵ(Fe) in HD 50264. The calculation was done with the adopted model $T_{\rm eff}$ = 5800 K, log g = 4.2, ϵ(Fe) = 7.18 and ξ = 1.0 km s^{-1}. The absence of any trend of the individual abundance with excitation potential and microturbulence shows that a correct value for $T_{\rm eff}$ and microturbulence velocity was chosen.

the error introduced by the microturbulence is quite significant. The uncertainties due to equivalent width errors affect only the abundances of elements, that are based on weak lines such as zirconium and cobalt in both stars. For the elements analyzed via spectrum synthesis the same technique was used, varying $T_{\rm eff}$, log g and ξ, then computing independently the abundance changes introduced by the variation of the above atmospheric parameters. They are also included in Tables 5 and 6.

4. Discussion

4.1. The abundance pattern of HD 50264 & HD 87080

Below we discuss the abundance pattern comparing with previous studies done for CH subgiants. Figures 3 and 4 show the abundance pattern of the two stars analyzed in this work. We are going to compare our abundance analysis with the results obtained by Smith et al. (1993) (hereafter SCL93), Luck & Bond (1991) (hereafter LB) and North et al. 1994.

4.1.1. α elements, iron group, Na and Al

The abundance of α-elements (Mg, Si, Ca and Ti) of the stars analyzed in this work has the same trend as a disk dwarf stars of same metallicity analyzed by Edvardsson et al. (1993) hereafter (E93). The mean of [Mg/Fe], [Si/Fe], [Ca/Fe] and [Ti/Fe] for a metallicity of −0.3 and −0.5 is +0.1, ≈+0.1, 0.0 and +0.1 (E93). The [α/Fe] mean given by [<Mg, Si, Ca, Ti>/Fe] for HD 50264 and HD 87080 is 0.07 and 0.16. Similar values were found for the sample stars analyzed in SCL93 and LB, 0.14 (taking into consideration only silicon and calcium; SCL93) and 0.18 (LB).

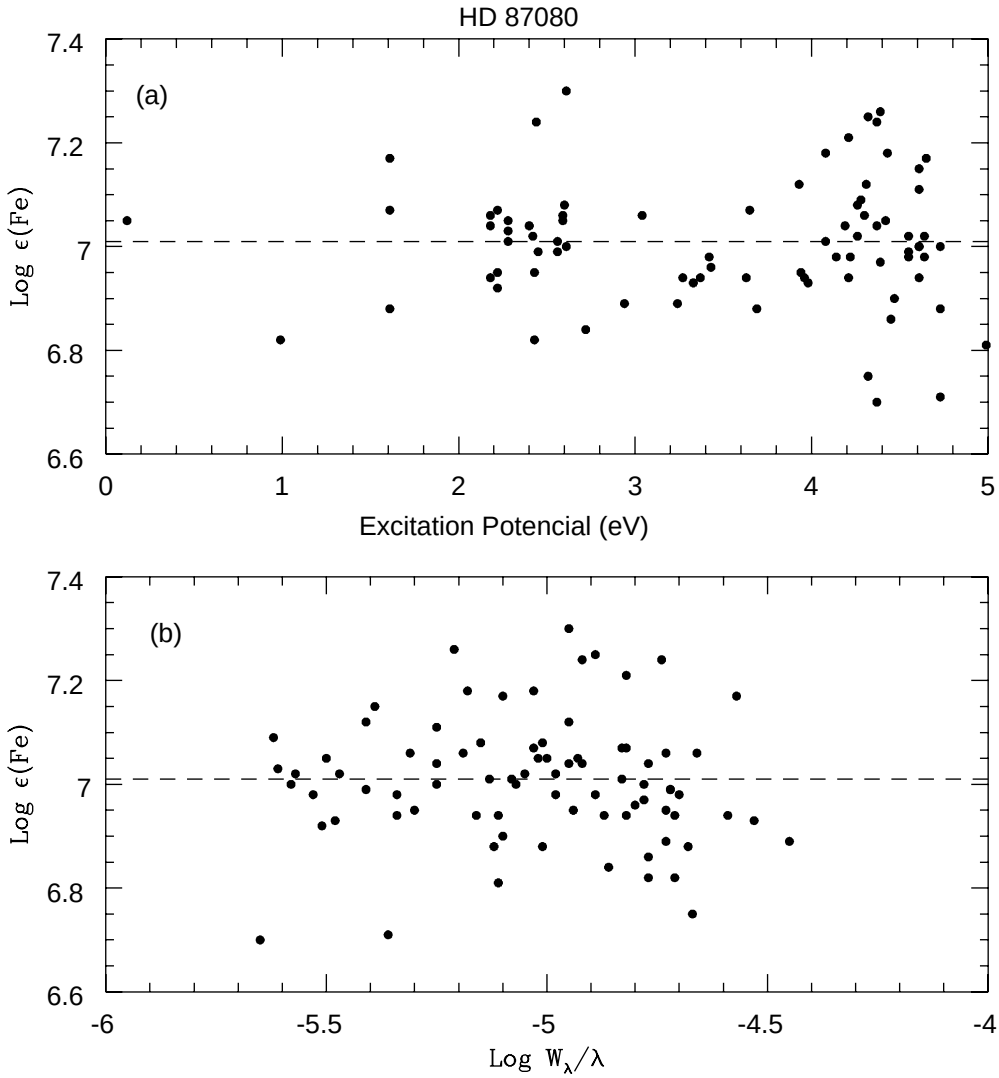

Fig. 2. The abundance of Fe by number ϵ(Fe) versus excitation potential (diagram **a)**) and the abundance of Fe by number ϵ(Fe) versus log (W_λ/λ) (diagram **b)**) for the 96 lines of Fe I,II employed in the determination of $T_{\rm eff}$, ξ and ϵ(Fe) in HD 87080. The calculation was done with the adopted model $T_{\rm eff}$ = 5600 K, log g = 4.0, ϵ(Fe) = 7.01 and ξ = 1.2 km s^{-1}. The absence of any trend of the individual abundance with excitation potential and microturbulence shows that a correct value for $T_{\rm eff}$ and microturbulence velocity was chosen.

The iron group elements Sc and V follow Fe. Cobalt and chromium in both stars show small enhancements. Nickel is basically solar. Our mean abundance for the iron group for HD 50264 and HD 87080 is 0.12 and 0.11, which is similar to other determinations for CH subgiant stars, 0.06 (SCL93) and 0.08 (LB). Manganese is also similar when compared to the two references above. Again, for HD 50264 and HD 87080 the values are 0.04 and −0.09, which is similar to the value given by SCL93 of 0.09.

The rest of the elements within the iron group, as well as zinc and copper either have small enhancements, as is the case for zinc for the two stars (HD 50264, 0.29; HD 87080, 0.26), or is solar, as is the case for copper (HD 50264, 0.04; HD 87080, 0.01). Copper and zinc were respectively, analyzed by SCL93 and LB with a mean of 0.00 ± 0.28 and 0.11 ± 0.12. A previous analysis of Cu and Zn in metal-poor dwarfs and giants using the 5782 Å Cu I and 4810 Å Zn I lines, was done by Sneden et al. (1991). That study found a mean solar [Cu/Fe] ratio for a metallicity range of $0.0 \geq$ [Fe/H] ≥ -1.0. The ratio [Zn/Fe] is solar, with a scatter of ≈0.1 dex in any metallicity range. Here our values confirm this trend copper has the solar value in the stars analyzed in this work. Zinc in our stars is slight enriched and marginally follows the tendency observed by Sneden et al. (1991).

Sodium and aluminun show the same trend as for disk dwarf stars with a mean of 0.1 for [Na/Fe] and [Al/Fe] for a −0.3 and −0.5 metallicity star (E93).

The abundance of europium for HD 50164 and HD 87080 lies slighty above the tendency seen in Fig. 13 of Woolf et al. (1995). In that plot, the [Eu/Fe] ratio for the disk and halo dwarf stars are plotted versus the metallicity. In that figure, the mean value of [Eu/Fe] for a metallicity of ≈−0.4 is 0.4.

4.1.2. Carbon and s-process elements

We now compare the carbon and s-process abundances of the stars analyzed here with other classes of peculiar binary

Table 4. Abundances in the scale log ϵ(H) = 12.0 and in the notation [X/Fe].

	HD 50264			HD 87080		
Species	n	log ϵ	[X/Fe]	n	log ϵ	[X/Fe]
Fe I	47	7.18 ± 0.08	—	81	7.01 ± 0.12	—
Fe II	15	7.15 ± 0.07	—	15	7.03 ± 0.09	—
C I	4	8.80 ± 0.06	+0.59	4	8.65 ± 0.23	+0.61
Na I	2	6.04	+0.05	2	5.82	0.00
Mg I	2	7.19	−0.05	2	7.17	+0.10
Al I	2	5.93	+0.01	2	5.89	+0.14
Si I	3	7.39 ± 0.30	+0.18	2	7.25	+0.21
Ca I	6	6.11 ± 0.14	+0.09	6	5.92 ± 0.07	+0.07
Sc II	5	2.72 ± 0.11	−0.36	5	2.78 ± 0.12	−0.13
Ti I	3	4.74 ± 0.09	+0.06	3	4.76 ± 0.24	+0.25
V I	—	—	—	2	3.41	−0.08
Cr I	3	5.48 ± 0.12	+0.15	3	5.37 ± 0.11	+0.21
Mn I	1	5.09	+0.04	1	4.79	−0.09
Co I	3	4.82 ± 0.20	+0.24	3	4.66 ± 0.21	+0.25
Ni I	3	5.86 ± 0.05	−0.05	4	5.78 ± 0.11	+0.04
Cu I	1	3.91	+0.04	1	3.71	+0.01
Zn I	2	4.55	+0.29	2	4.35	+0.26
Rb I	1	2.65	+0.34	1	2.80	+0.71
Y II	6	2.78 ± 0.13	+0.88	6	2.74 ± 0.19	+1.01
Zr I	3	3.55 ± 0.33	+1.29	2	3.31 ± 0.04	+1.22
Ba II	1	3.04	+1.25	1	3.13	+1.51
La II	3	1.75 ± 0.30	+0.92	3	2.41 ± 0.06	+1.75
Ce II	5	2.00 ± 0.19	+0.76	4	2.39 ± 0.20	+1.32
Nd II	4	1.63 ± 0.17	+0.47	6	1.96 ± 0.12	+0.97
Eu II	1	0.61	+0.44	1	0.61	+0.61

systems with s-process enhancements: CH subgiants, barium giants, metal-deficient-barium stars, yellow-symbiotics and CH stars. Inspection of Figs. 3 and 4 reveals that HD 50264 and HD 87080 show a general overabundance of elements heavier than Rb synthesized by neutron capture. The available abundances for low-metallicity dwarf stars (E93) indicate that the chemical evolution of the Galaxy cannot be responsible for the s-process overabundances observed in these stars.

The abundance pattern of HD 50264 and HD 87080 implies a mean heavy s-process [s/Fe] elements excess for Y, Zr, Ba, La, Ce and Nd of, respectively 0.93 and 1.3. Similar values are found among other studies already done for CH subgiants; SCL93, LB and North et al. (1994). Figures 5 and 6 show [s/Fe] versus [Fe/H] and [hs/ls] versus [Fe/H] for a sample of several binary systems that are s-process enriched, classical barium-stars, CH subgiants, CH stars, yellow-symbiotics, metal-deficient Ba stars and the two stars analyzed in this work. We also include the star HD 196944 although its status is still not clear; it could be a AGB star or a CH star (Zacs et al. 1998). Figures 5 and 6 show that the parameters [s/Fe] and [hs/ls] are anticorrelated with metallicity and the scatter in these two relations increases for metallicity values less −1.0. The positions of the two CH subgiants analyzed in this work, in both plots, is the same as the other stars of the same class. As Clayton (1988) has shown, the clear significant trend of increasing [hs/ls] (as well as [s/Fe]) with decreasing metallicity is the result of the operation of the reaction $^{13}C(\alpha,n)^{16}O$ as a neutron source. Figures 5 and 6 illustrate very clear such behavior.

As the [hs/ls] and [s/Fe] index are anticorrelated with metallicity, the carbon abundance is also anticorrelated. Figure 7 shows [C/Fe] versus [Fe/H] for a sample of barium giants and dwarfs, CH subgiants and CH stars. Symbols have their usual meaning as in Figs. 5 and 6. Figure 8 shows how the carbon abundance is correlated with the abundance of the s-process elements. The barium stars, both giants and dwarfs, are concentrated in a region around [s/Fe] ≈ 1.0 and [C/Fe] ≈ 0.5, while the CH stars as well as HD 196144 (Zacs et al. 1998), have higher [C/Fe] and [s/Fe] ratios. Clearly more objects with higher [C/Fe] (CH stars for example) are needed to be observed in order to reduce the scatter seen in this figure for [C/Fe] larger than 1.0.

We can use the abundance of the s-process elements to determine the neutron exposure τ in order to characterize the s-process efficiency. We have calculated the heavy-element abundance excess in the two stars and then compared with the theoretical values calculated by Malaney (1987a,b). Before get into the details of the s-process distribution we must first correct the observed abundances for the initial heavy-element

Table 5. Abundance uncertainties of HD 50264. The second column gives the variation of the abundance ratios caused by a +0.08 dex variation in [Fe/H], the third column gives the variation of the abundance ratios caused by a +100 K variation in $T_{\rm eff}$. The other columns refer to variations due to: $\Delta \log g = +0.2$, $\Delta\xi = +0.3$ km s^{-1}. The W_λ and gf uncertainties are discussed in the text. The seventh column gives the compounded rms uncertainty of the second to sixth columns.The last column gives the observed abundance dispersion of those elements with more than three available lines.

Species	Δ[Fe/H]	Δ $T_{\rm eff}$	Δ log g	Δ ξ	Δ W_λ	$\left(\sum \sigma^2\right)^{1/2}$	$\sigma_{\rm obs}$
Fe I	0.00	+0.09	+0.01	+0.06	+0.04	0.18	0.09
Fe II	+0.03	−0.06	+0.12	+0.03	+0.04	0.14	0.13
C I	0.00	−0.07	+0.06	0.00	+0.09	0.14	0.06
Na I	0.00	+0.06	+0.01	−0.01	+0.08	0.20	—
Mg I	0.00	+0.05	+0.04	−0.01	+0.14	0.18	—
Al I	−0.01	+0.09	0.00	0.00	+0.11	0.22	—
Si I	0.00	+0.03	+0.01	−0.01	+0.06	0.18	0.30
Ca I	−0.01	+0.07	−0.03	−0.06	+0.05	0.12	0.14
Sc II	+0.03	+0.01	+0.07	−0.04	+0.06	0.16	0.11
Ti I	−0.01	+0.09	0.00	−0.02	+0.10	0.14	0.09
Cr I	−0.01	+0.08	0.00	−0.01	+0.00	0.12	0.12
Mn I	+0.01	+0.10	0.00	+0.10	+0.05	0.18	—
Co I	−0.01	+0.09	+0.01	−0.01	+0.13	0.25	0.20
Ni I	−0.01	+0.09	+0.01	−0.03	+0.07	0.15	0.05
Cu I	+0.01	+0.05	0.00	0.00	+0.05	0.12	—
Zn I	+0.02	+0.04	+0.01	−0.16	+0.07	0.25	—
Rb I	0.00	+0.05	0.00	+0.10	+0.05	0.23	—
Y II	+0.04	+0.03	+0.06	−0.13	+0.08	0.18	0.13
Zr I	−0.01	+0.12	+0.01	0.00	+0.18	0.28	0.33
Ba II	+0.02	+0.05	−0.01	−0.08	+0.01	0.20	—
La II	+0.04	+0.03	+0.08	−0.02	+0.10	0.23	0.30
Ce II	+0.04	+0.03	+0.08	−0.03	+0.12	0.27	0.19
Nd II	+0.13	+0.03	+0.08	−0.01	+0.14	0.27	0.17
Eu II	+0.01	0.00	+0.10	0.00	+0.05	0.11	—

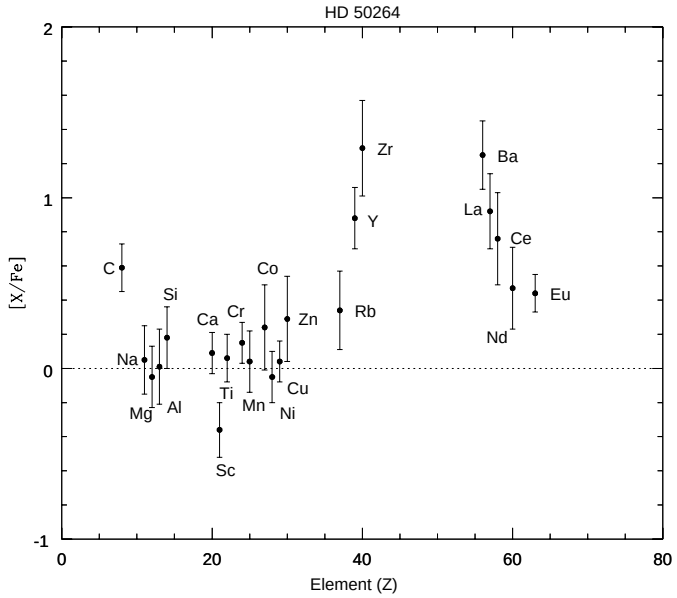

Fig. 3. Abundance pattern of HD 50264. The error bars were taken from Col. 7 in Table 5 and represent the combined errors for each element.

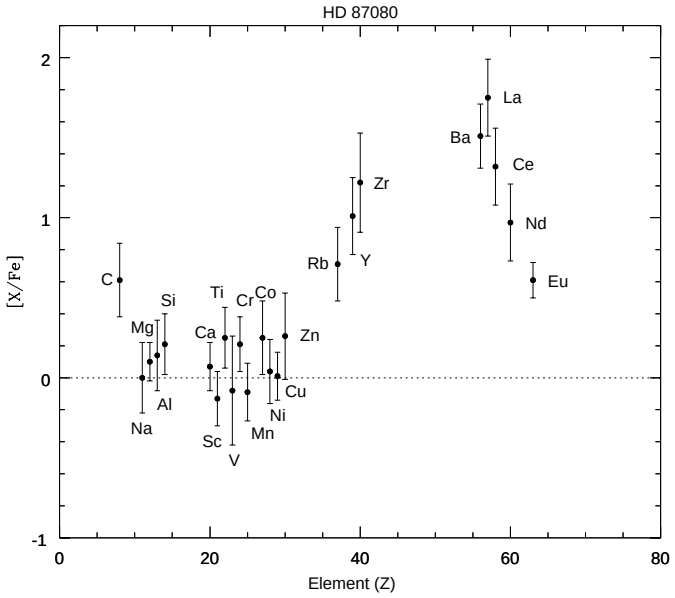

Fig. 4. Abundance pattern of HD 87080. The error bars were taken from Col. 7 in Table 6 and represent the combined errors for each element.

Table 6. Abundance uncertainties of HD 87080. The second column gives the variation of the abundance ratios caused by a +0.12 dex variation in [Fe/H], the third column gives the variation of the abundance ratios caused by a +150 K variation in $T_{\rm eff}$. The other columns refer to variations due to: $\Delta \log g = +0.2$, $\Delta\xi = +0.4$ km s^{-1}. The W_λ and gf uncertainties are discussed in the text. The seventh column gives the compounded r.m.s. uncertainty of the second to sixth columns.The last column gives the observed abundance dispersion of those elements with more than three available lines.

Species	Δ[Fe/H]	Δ $T_{\rm eff}$	Δ log g	Δ ξ	Δ W_λ	$\left(\sum \sigma^2\right)^{1/2}$	$\sigma_{\rm obs}$
Fe I	0.00	+0.12	+0.01	−0.11	+0.06	0.18	0.12
Fe II	−0.02	−0.04	−0.07	−0.07	+0.08	0.14	0.09
C I	0.00	−0.15	−0.06	0.00	+0.12	0.21	0.23
Na I	0.00	+0.08	0.00	−0.01	+0.09	0.22	—
Mg I	0.00	+0.05	+0.04	−0.02	+0.04	0.12	—
Al I	0.00	+0.08	0.00	−0.01	+0.12	0.22	—
Si I	0.00	+0.04	−0.01	−0.01	+0.09	0.19	—
Ca I	0.00	+0.10	+0.01	−0.08	+0.07	0.15	0.07
Sc II	−0.02	+0.01	−0.07	−0.06	+0.09	0.17	0.12
Ti I	0.00	+0.15	0.00	−0.02	+0.11	0.19	0.24
V I	−0.01	+0.15	−0.01	−0.02	+0.14	0.34	—
Cr I	0.00	+0.12	0.00	−0.02	+0.11	0.17	0.11
Mn I	+0.01	+0.10	0.00	−0.10	+0.05	0.18	—
Co I	−0.01	+0.15	−0.02	−0.01	+0.17	0.23	—
Ni I	0.00	+0.14	−0.01	−0.06	+0.09	0.20	0.11
Cu I	+0.01	+0.10	0.00	0.00	+0.04	0.15	—
Zn I	−0.02	+0.03	−0.02	−0.17	+0.09	0.27	—
Rb I	0.02	+0.05	−0.05	−0.15	+0.05	0.23	—
Y II	−0.03	+0.02	−0.06	−0.20	+0.10	0.24	0.15
Zr I	0.00	+0.19	−0.01	−0.01	+0.16	0.31	—
Ba II	+0.02	+0.07	0.00	+0.08	+0.03	0.20	—
La II	−0.03	+0.04	−0.07	−0.12	+0.10	0.24	0.06
Ce II	−0.03	+0.03	−0.07	−0.11	+0.11	0.24	0.20
Nd II	+0.04	+0.02	−0.09	−0.05	+0.11	0.24	0.12
Eu II	+0.01	0.00	+0.10	0.00	+0.05	0.11	—

distribution. We corrected our observed abundances, $\epsilon_{\rm obs}$, to the actual s-process overabundances, $\epsilon'_{\rm s}$ by using the following relation

$$\epsilon'_{\rm s} = \epsilon_{\rm obs} - \epsilon_{\rm i} \quad (3)$$

in which $\epsilon_{\rm i}$ is equal to solar-system heavy-element abundances scaled to HD 50264 and HD 87080 metallicities assuming $[{\rm s/Fe}]_{\rm i} \approx 0.0$. Table 7 summarizes the values of $\log \epsilon_{\rm obs}$, $\log \epsilon_{\rm i}$ and $\log \epsilon'_{\rm s}$ for the heavy elements.

For europium, which is primarily an r-process element with a different chemical history than the s-process elements, we used the results of Woolf et al. (1995) to estimate the initial abundance, taking $[{\rm Eu/Fe}]_{\rm i} = +0.1$ and +0.2 for HD 50264 and HD 87080.

According to Malaney, the s-process efficiency can be obtained using the abundance tables for s-process nucleosynthesis. These tables list element abundance enhancements for elements either exposed to a single neutron exposure (Malaney 1987a) or to an exponential distribution, $\exp(-\tau/\tau_0)$, of neutron exposures τ (Malaney 1987b).

In order to quantify the comparison between the observations and models, we used the "goodness of the fit" criterion as defined by Cowley & Downs (1980) and often used in the literature, Smith (1984), van Winckel & Reyners (2000):

$$S^2 = \frac{1}{N}\sum_{i=1}^{N}\frac{(O_i - P_i)^2}{{\sigma_i}^2} \quad (4)$$

where N is the number of the elements involved in the comparison, $O_{\rm i}$ is the observed abundance of the element i, P_i is the predicted model abundance of element i and σ_i is the uncertainty in the observed abundance of the element i. The values of the $\sigma_{\rm i}$ were taken from the quadratic average values in Tables 5 and 6 (column labeled $\left(\sum \sigma^2\right)^{1/2}$). The values for S^2 and τ are given in Table 8 for models corresponding to a single exposure. Single neutron exposure models with $N_{\rm n} = 10^8$ cm^{-3} provided a better fit (i.e. smaller S^2) to the observed abundances than models with exponential distributions. Table 8 shows that the two stars are very similar both in the neutron exposure as well as in the neutron density. This is not surprising given the similarities in the abundance distributions of HD 50264 and HD 87080. Figure 9 shows the plot of the s-process abundances in HD 50264 and in HD 87080 and Malaney's (1987a) model predictions for $\tau = 0.9$ and 1.0, respectively for HD 50264 and HD 87080, and $N_{\rm N} = 10^8$ cm^{-3}. There is a good agreement, for the two stars, between the model predictions and the observed abundances. The abundance of europium shows a modest disagreement with model predictions, since europium has a strong r-process component and its initial abundance could be different from our assumption of $[{\rm Eu/Fe}]_{\rm i} = +0.1$ and +0.2 for HD 50264 and HD 87080.

The values of the neutron exposure, τ, versus metallicity is plotted in Fig. 10 for several classes of binary stars that are s-process enriched. In that plot the neutron exposure is

Table 7. Comparison between observed heavy-element abundances in HD 50264 and HD 87080 and parametrized s-process model predictions for single exposure and $N_N = 10^8$ cm^{-3}.

	HD 50264				HD 87080			
Species	log ϵ_{obs}	log ϵ_i	log ϵ_s'		log ϵ_{obs}	log ϵ_i	log ϵ_s'	
			obs	model			obs	model
Rb	2.65	2.30	2.38	2.26	2.80	2.29	2.64	2.19
Y	2.78	2.44	2.51	2.67	2.74	2.23	2.58	2.60
Zr	3.55	3.21	3.28	3.13	3.31	2.80	3.15	3.11
Ba	3.04	2.70	2.77	2.78	3.13	2.62	2.97	3.10
La	1.75	1.41	1.48	1.50	2.41	1.90	2.25	1.89
Ce	2.00	1.66	1.73	1.76	2.39	1.88	2.23	2.22
Nd	1.63	1.36	1.36	1.24	1.96	1.45	1.80	1.75
Eu	0.61	0.27	0.34	−0.61	0.61	0.30	0.30	−0.07

Table 8. τ and S^2 values for single exposure models and for $N_N = 10^8$ cm^{-3}.

HD 50264					HD 87080				
		τ					τ		
1.1	1.0	0.9	0.8	0.7	1.2	1.1	1.0	0.9	0.8
		S^2					S^2		
11.48	3.52	0.24	6.38	21.78	5.23	2.03	0.41	5.48	21.06

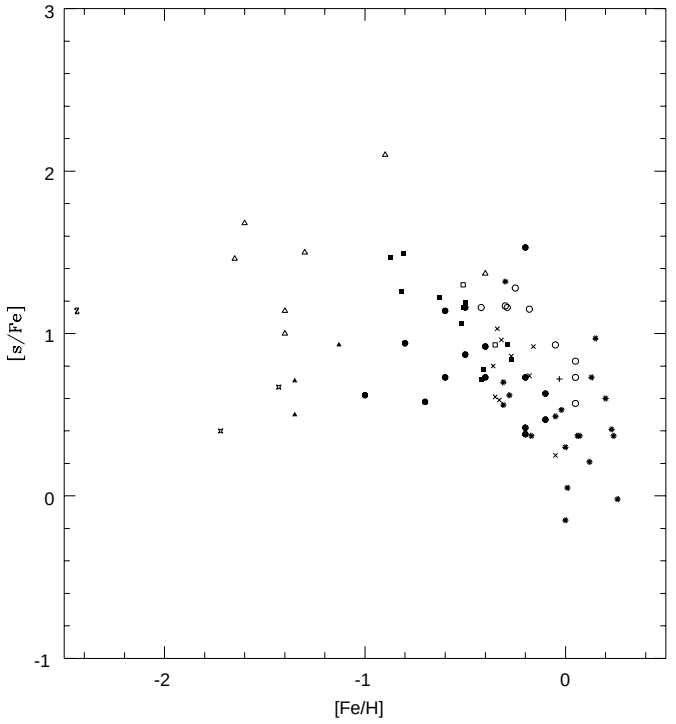

Fig. 5. Diagram of the mean s-process elements given by the ratio [s/Fe] as a function of the metallicity for a sample of s-process enriched objects. CH subgiant stars analyzed in this work, open squares; barium dwarfs from North et al. (1994), filled squares; CH subgiants from SCL93, diagonal crosses; CH subgiants from LB, filled circles; barium giants from Smith (1984) and from Kovacs (1985), open circles; barium giants from Zacs (1994), asterisks; metal-deficient barium stars from Junqueira & Pereira (2001), stars; CH stars from Vanture (1992c), open triangles; yellow-symbiotics from Smith et al. (1996, 1997) and Pereira et al. (1998), filled triangles; and ζ Cap from Smith et al. (1980), crosses and HD 196944, Z (Zacs et al. 1998).

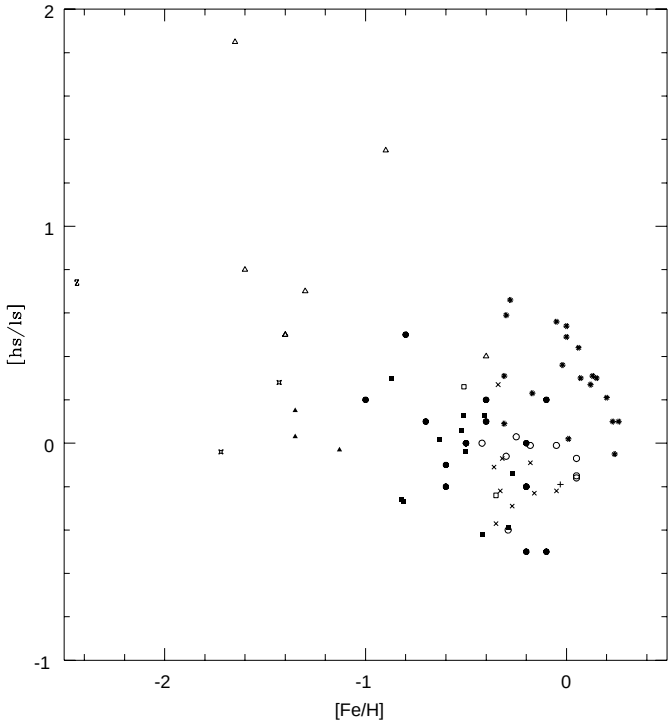

Fig. 6. Diagram of the neutron exposure parameter estimator [hs/ls] as a function of the metallicity for a sample of binary systems that is s-process enriched. The symbols have the same meaning as in Fig. 5.

anti-correlated with metallicity. If the same correlation with the [hs/ls]-index versus metallicity is seen for this kind of objects (Fig. 6 of this work), then τ increases as the [hs/ls] increases (van Winckel & Reyniers 2000). This kind of relation is another argument in favor the reaction of $^{13}C(\alpha,n)^{16}O$ as a neutron source.

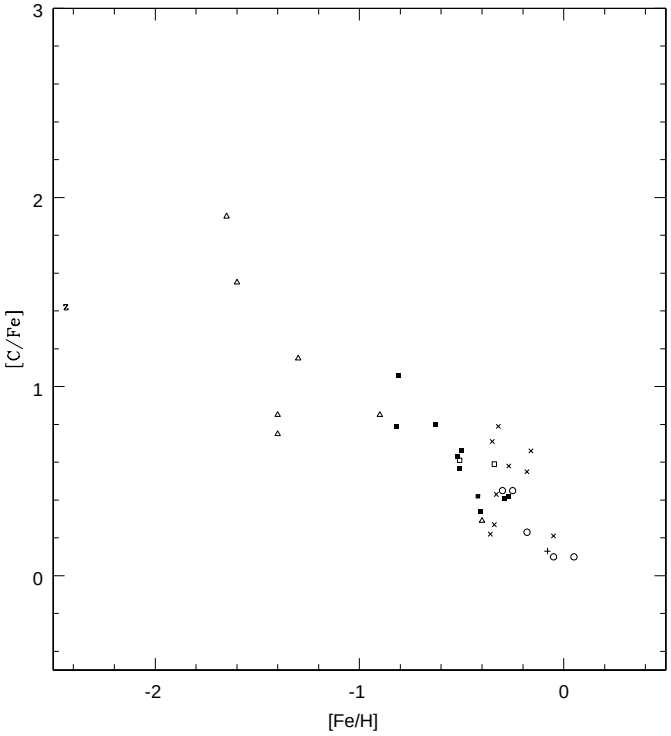

Fig. 7. Diagram of of [C/Fe] ratio versus metallicity. The symbols have the same meaning as in Fig. 5.

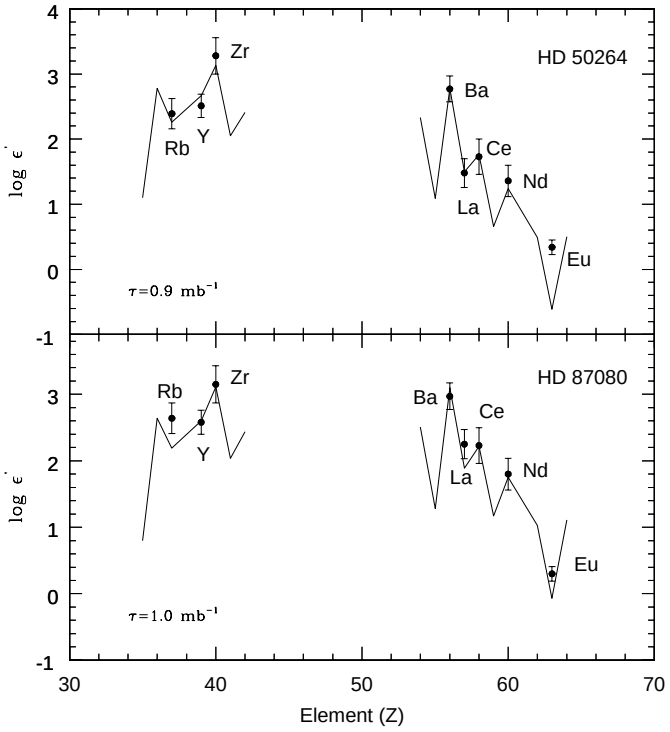

Fig. 9. Comparison of the s-process component in the observed abundances log ϵ' (dots) with model predictions from Malaney (1987a) for a single exposure and a neutron density of $N_n = 10^8$ cm^{-3}.

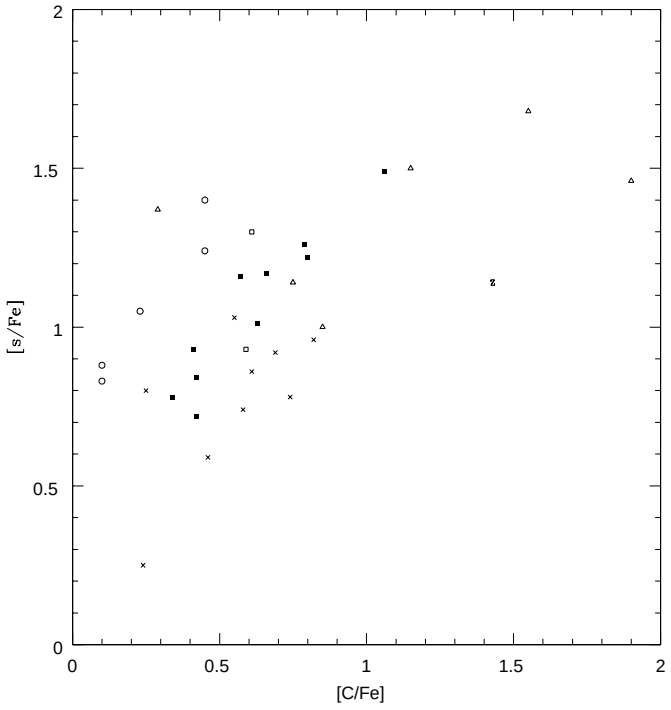

Fig. 8. Diagram of the mean s-process elements given by the ratio [s/Fe] as a function of [C/Fe] for a sample of binary systems s-process enriched. The symbols have the same meaning as in Fig. 5.

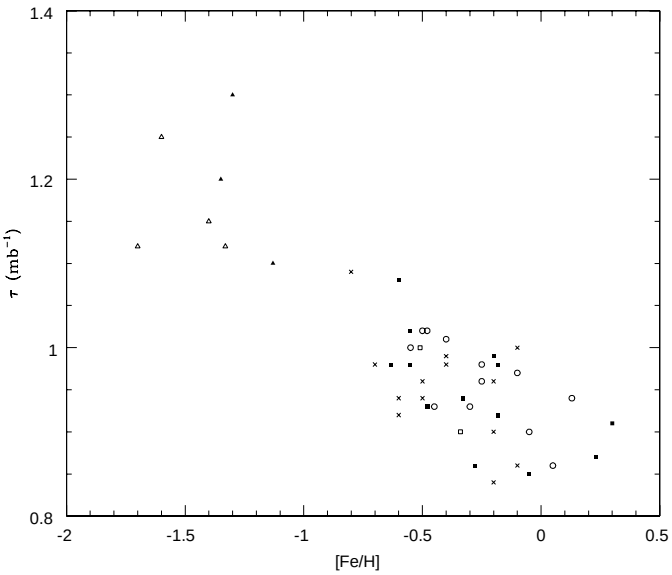

Fig. 10. The neutron exposure, τ, versus metallicity for several classes of binary systems that are s-process enriched. The symbols have the same meaning as in Fig. 5.

The abundance of rubidium can provide other insights into the s-process environment in HD 50264 and in HD 87080. In Fig. 11 we show the s-process ratio of log [N(Rb)/N(Zr)] versus [Fe/H] for barium giants (Tomkin & Lambert 1983; Smith & Lambert 1984; Malaney & Lambert 1988) yellow symbiotics (Smith et al. 1996, 1997 and Pereira et al. 1998) and the two stars analyzed in this work. The position of HD 50264 and HD 87080 also strengthens the trend of increasing neutron densities with decreasing metallicities.

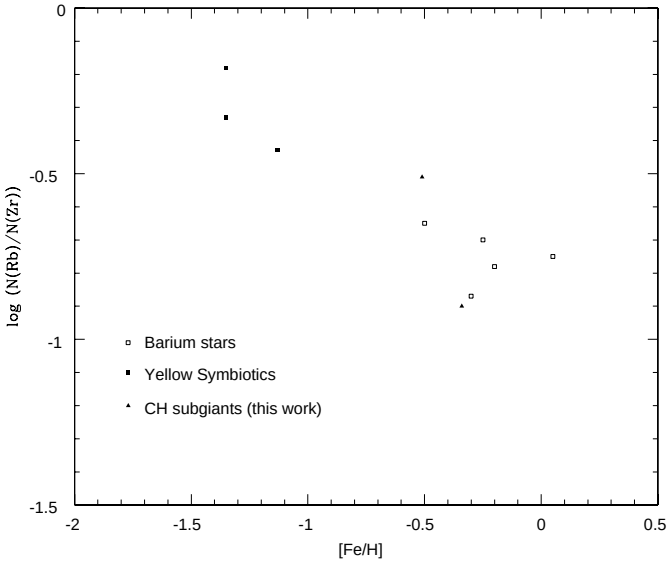

Fig. 11. S-process log [N(Rb)/N(Zr)] ratio for heavy-element enriched stars. The barium stars are from Tomkin & Lambert (1983); Smith & Lambert (1984); Malaney & Lambert (1988); the yellow-symbiotics from Smith et al. (1996, 1997) and Pereira et al. (1998) and the two CH subgiant stars analyzed in this work.

5. Conclusions

An abundance analysis, employing high-resolution optical spectra, of the two CH subgiant stars reveal them enriched substantially in the heavy s-process elements. The abundance pattern for the iron peak elements, α group as well as sodium and aluminum follow the disk abundance. With respect to s-process nucleosynthesis, we compare these two stars analyzed here with several binary systems that display s-process enrichment. In all plots showed in this work, involving several relations among [hs/ls]-, [s/Fe]- and τ-index, metallicity and [C/Fe] ratio, both HD 50264 and HD 87080 display values that fit well the observed behavior of other CH subgiant stars. Besides, the ratio [Rb/Zr] was also obtained and it was compared with other classes of chemically peculiar binary systems. Although the two stars analyzed here can add a few points in the diagram log [Rb/Zr] versus metallicity, they also represent further evidence for reaction $^{13}C(\alpha,n)^{16}O$ as a neutron source.

References

Biémont, E., & Godefroid, M. 1980, Phys. Scr., 22, 231
Biémont, E., Grevesse, N., Hannaford, P., & Lowe, R. M. 1981, ApJ, 248, 867
Biémont, E., Karner, C., Meyer, G., Traeger, F., & Zu Putlitz, G. 1982, A&A, 107, 166
Blackwell, D. E., Menon, S. L. R., & Petford, A. D. 1983, MNRAS, 204, 883
Blackwell, D. E., Booth, A. J., Menon, S. L. R., & Petford, A. D. 1986, MNRAS, 220, 289
Bond, H. E. 1974, ApJ, 194, 95
Booth, A. J., Shallis, M. J., & Wells, M. 1983, MNRAS, 205, 191
Catchpole, R. M., Robertson, B. S. C., & Warren, P. R. 1977, MNRAS, 181, 391
Clayton, D. 1988, MNRAS, 234, 1
Cowley, C. R., & Downes, P. L. 1980, ApJ, 236, 648
Drake, J. J., & Smith, G. 1991, MNRAS, 250, 89
Edvardsson, B., et al. 1993, A&A, 275, 101 (E93)
Hannaford, P., Lowe, R. M., Grevesse, N., Biemont, E., & Whaling, W. 1982, ApJ, 261, 736
Iben, I., & Renzini, A. 1983, ARA&A, 21, 271
Jaschek, C., et al. 1985, The absolute magnitudes of barium stars, ed. M. Jaschek, & P. C. Keenan, in Cool stars with excess of heavy elements (Dordrecht: D. Reidel Publ. Co.) 185
Junqueira, S., & Pereira, C. B. 2001, AJ, 122, 360
Kaufer, A., Stahl, S., Tubbesing, S., et al. 1999, The Messenger, 95, 8
Koch, M., & Richter, J. 1968, Zs. für Ap., 69, 180
Kovacs, N. 1985, A&A, 150, 232
Krishnaswany, K., & Sneden, C. 1985, PASP, 97, 407
Kurucz, R. L. 1993, CD-ROM 13, Atlas9 Stellar Atmosphere Programs and 2 km/s Grid (Cambridge: Smithsonian Astrophys. Obs.)
Kurucz, R. L. 1994, CD-ROM, 20-22
Lambert, D. L., & Luck, R. E. 1978, MNRAS, 183, 79
Lambert, D. L., Roby, S. W., & Bell, R. A. 1982, ApJ, 254, 664
Lambert, D. L. 1985, The chemical composition of cool stars. I - The barium stars, ed. M. Jaschek, & P. C. Keenan, in Cool stars with excess of heavy elements (Dordrecht: D. Reidel Publ. Co.), 191
Lambert, D. L. 1988, Chemical composition as a signature of stellar evolution - The Barium stars, de strobel, ed. G. Cayrel, & M. Spite, in The impact of very high S/N spectroscopy on Stellar Physics. IAU Symp. 132, 563
Lambert, D. L., et al. 1996, ApJS, 103, 183
Lawler, J. E., & Dakin, J. T. 1989, J. Opt. Soc. Am. B, 6, 1457
Lu., P. K., et al. 1983, ApJS, 52, 169
Luck, R. E., & Bond, H. E. 1985, ApJ, 292, 559
Luck, R. E., & Bond, H. E. 1991, ApJS, 77, 515 (LB)
MacConnel, D. J., Fyre, R. L., & Upgren, A. R. 1972, AJ, 77, 384
Malaney, R. A. 1987a, ApJ, 321, 832
Malaney, R. A. 1987b, Ap&SS, 137, 251
Malaney, R. A., & Lambert, D. L. 1988, MNRAS, 235, 695
Martin, G. A., Fuhr, J. R., & Wiese, W. L. 1988, J. Phys. Chem. Ref. Data, 17, 4
McClure, R. D., Fletcher, J. M., & Nemec, J. M. 1980, ApJ, 238, L35
McClure, R. 1997, PASP, 109, 536
Mennessier, M. O., et al. 1997, A&A, 326, 722
North, P., Berthet, S., & Lanz, T. 1994, A&A, 281, 775
North, P. 1995, Mem. Soc. Astron. Ital., 66, 379
Pereira, C. B., Smith, V. V., & Cunha, K. 1998, AJ, 116, 1977
Schmidt-Kaler, T. 1982, in Landolt-Börnstein New Series, ed. K. Schaifers, & H. H. Vigt, Group 4, Vol. 2b (Berlin: Springer), 449
Smith, G., Edvardsson, B., & Frisk, U. 1986, A&A, 165, 126
Smith, V. V., Sneden, C., & Pilachowski, C. A. 1980, PASP, 92, 809
Smith, V. V., & Lambert, D. L. 1984, PASP, 96, 226
Smith, V. V. 1984, A&A, 132, 326
Smith, V. V., & Lambert, D. L. 1986, ApJ, 311, 843
Smith, V. V., Coleman, H., & Lambert, D. L. 1993, ApJ, 417, 287 (SCL93)
Smith, V. V., et al. 1996, A&A, 315, 179
Smith, V. V., et al. 1997, A&A, 324, 97
Sneden, C. 1973, Ph.D. Thesis, Univ. of Texas
Sneden, C., Gratton, R. G., & Crocker, D. A. 1991, A&A, 246, 354
Tomkin, J., & Lambert, D. L. 1983, 273, 722
Vanture, A. 1992c, AJ, 104, 1997
van Winckel, H., & Reyniers, M. 2000, A&A, 345, 135
Vandenberg, D. 2000, ApJS, 532, 430
Wiese, W. L., Smith, M. W., & Miles, B. M. 1969, NBS Ref. Data. Ser.
Wiese, W. L., & Martin, G. A. 1980, NSDRS-NBS, 68
Woolf, V. M., Tomkin, J., & Lambert, D. L. 1995, ApJ, 453, 660
Youssef, N. M., & Amer, M. A. 1989, A&A, 220, 281
Zacs, L. 1994, A&A, 283, 937
Zacs, L., Nissen, P. E., & Schuster, W. J. 1998, A&A, 337, 216